Phys. 40, 1265 (1964).
[16]A. Skerbele and E. N. Lassettre, J. Chem. Phys. 45, 1077 (1966).
[17]E. N. Lassettre, A. Skerbele, and V. D. Meyer, J. Chem. Phys. 45, 3214 (1966).
[18]J. Geiger, Z. Physik 175, 530 (1963).
[19]L. Vriens, J. Arol Simpson, and S. R. Mielczarek, Phys. Rev. 165, 7 (1968).
[20]Y.-K. Kim and M. Inokuti, Phys. Rev. 175, 176 (1968).
[21]Y.-K. Kim and M. Inokuti, Phys. Rev. 184, 38 (1969).
[22]K. L. Bell, D. J. Kennedy, and A. E. Kingston, J. Phys. B 2, 26 (1969).
[23]A. Weiss (private communication).
[24]K. L. Bell, D. J. Kennedy, and A. E. Kingston, J. Phys. B 1, 1028 (1968).
[25]W. Oldham, Phys. Rev. 186, 52 (1969).
[26]G. Peach (private communication).
[27]Y.-K. Kim, M. Inokuti, G. E. Chamberlain, and S. R. Mielczarek, Phys. Rev. Letters 21, 1146 (1968).
[28]Y.-K. Kim (private communication).
[29]A. Skerbele and E. N. Lassettre, J. Chem. Phys. 52, 2708 (1970).
[30]M. Inokuti, Rev. Mod. Phys. 43, 297 (1971); Y.-K. Kim and M. Inokuti, in *Electronic and Atomic Collisions*, edited by L. Branscomb *et al.* (North-Holland, Amsterdam, 1971), p. 762.
[31]I. V. Hertel and K. J. Ross, J. Phys. B 2, 285 (1969).
[32]I. V. Hertel and K. J. Ross, J. Phys. B 2, 484 (1969).
[33]R. H. Garstang, J. Phys. B 1, 847 (1968).
[34]E. N. Lassettre, A. Skerbele, and M. A. Dillon, J. Chem. Phys. 50, 1829 (1969).
[35]T. Sawada, J. E. Purcell, and A. E. S. Green, Bull. Am. Phys. Soc. 15, 1365 (1970).
[36]E. J. McGuire, Sandia Research Report SC-RR-70-46, 1971 (unpublished).

PHYSICAL REVIEW A VOLUME 5, NUMBER 2 FEBRUARY 1972

Differential Energy and Angular Cross Sections for Ionization by Several-Hundred-keV Electrons: Theory and Comparison with Experiment

John W. Cooper and H. Kolbenstvedt*
National Bureau of Standards, Washington, D. C. 20234
(Received 19 August 1971)

A procedure for calculating cross sections for ionization of electrons in various shells of an atom differential in both angle and final electron energy is developed. Calculations for ionization of carbon, copper, and gold for incident energies in the range 100–400 keV are presented and compared with recent experimental results.

I. INTRODUCTION

Interest in the low-energy spectra of electrons from scattering of electron beams of moderate energy (i.e., a few m_0c^2 or several MeV) was stimulated a number of years ago by Keiffer and Parzen,[1] who noted that a peak at low energies and large angle should appear in the energy spectrum due to electrons that have lost energy via Bremsstrahlung. Subsequent work[2,3] demonstrated rather conclusively that such a low-energy Bremsstrahlung peak would be completely masked by inelastic processes resulting in energy loss to bound electrons and by plural scattering even in very thin targets. A detailed experimental study of these processes at somewhat lower energies has now been made.[4] A number of new features have emerged from this work.

(i) For low-Z materials (where the incident energy is much larger than the K-shell binding energy) the prominent feature of the spectra observed at angles $<90°$ is the Møller peak corresponding to conservation of energy and momentum for free-electron scattering. However, broadening of these peaks due to binding effects is observable.

(ii) All spectra show a low-energy "tail" in addition to the Møller peak. At low incident energies and large scattering angles these contributions cannot be separated.

(iii) Low-energy electrons peak at 90° for high incident energies but this peak shifts to smaller angles as the incident energy is lowered.

(iv) For high-Z materials (Cu, Ag, Au) much broader peaks are observed. At low incident energies and moderately small angles there is a large component of scattering for final energies above the Møller energy.

In order to provide an understanding of these features, calculations of the energy spectra for all of the elements, initial energies, and final angles of observation reported in Ref. 4 have been performed. The method of calculation follows the general framework outlined in Ref. 2. However, it was necessary to remove some of the approximations made in Ref. 2, since they are no longer valid for incident energies in the 100–400 keV range, and

to extend the calculations to all atomic shells. The basic formalism, which can easily be adapted to other cases, is presented in Sec. II.

A detailed comparison between the experimental spectra obtained in Ref. 4 and these calculations are made in Sec. III (for carbon) and in Sec. IV (for gold and copper). This comparison indicates that the broadening of Møller peaks and the spectral behavior of the low-energy "tails" are qualitatively the same in both experimental and calculated results. Also, the angular dependence of low-energy electrons as a function of incident energy is similar in both determinations. However, no evidence for large contributions to scattering for energies above the Møller energy was obtained from the calculations. We attribute this disagreement between theory and experiment to plural scattering. A brief discussion of the effects of plural scattering on the experimental data is given in Sec. V. Also a discussion of the inadequacies of using plane waves to describe the free electrons in the theoretical treatment is included in Sec. V.

II. THEORY

Consider an electron of total energy ϵ_1, momentum $\vec{p}_1$, incident on an electron of binding energy I, and therefore total energy $\epsilon_2 = 1 - I$. Conservation of energy is given by the relation

$$\epsilon_1 + 1 - I = \epsilon_1' + \epsilon_2'$$

or (1)

$$E_1 - I = E_1' + E_2' ,$$

where $E_i = \epsilon_i - 1$ is the kinetic energy of electron i and where primes denote energy after ionization has taken place.[5]

The matrix element for ionization is given in Eq. (4) of Ref. 2 as

$$M = Ae^2 \int d\vec{r} \int d\vec{r}\,' (e^{i(\epsilon_1 - \epsilon_1')|\vec{r} - \vec{r}\,'|} / |\vec{r} - \vec{r}\,'|) \times \bar{\Psi}_{2'}(\vec{r})\gamma_\mu \Psi_2(\vec{r}) \bar{\Psi}_{1'}(\vec{r}\,')\gamma_\mu \Psi_1(\vec{r}\,') . \quad (2)$$

Here $\Psi_1(\vec{r})$ represents the total wave function (including spin of electron 1), γ_μ is the Dirac four-vector, and the asymmetry operator A indicates that the matrix element is to be antisymmetrized by evaluating it twice with the coordinates of $1'$ and $2'$ interchanged. In the following, ϵ_1' (or E_1') represents the energy of the detected electron by convention, whether or not this electron originates from the incident beam or has been ejected from the atom.

In terms of this matrix element the cross section for ionization in which a final electron of kinetic energy E_1' is observed in an angular range $d\Omega_1'$ is

$$\frac{d\sigma}{dE_1' d\Omega_1'} = \frac{(2\pi)^{-5} \epsilon_1 \epsilon_1' p_1'}{p_1} \times \int d\vec{p}_2' \sum |M|^2 \delta(\epsilon_1 + 1 - I - \epsilon_1' - \epsilon_2') . \quad (3)$$

Energy conservation [Eq. (1)] is implied by the δ function and $\sum$ implies that summation and averaging over spins in the final and initial states, respectively, is to be carried out in evaluating $|M|^2$. $\vec{p}_1$ is the momentum three-vector corresponding to E_i.

Equation (3) represents the ionization cross section within the following limitations: (a) Ionization is considered as a two body process, it being assumed that atomic binding effects and the interaction with other electrons can be accounted for by a suitable choice of initial- and final-state one-electron wave functions. (b) No radiative effects are included. Both of these restrictions are not expected to produce any serious error in the energy range considered here.

In order to evaluate Eq. (3), assumptions must be made about the wave functions $\Psi_i(\vec{r})$ used in evaluating the matrix element. We have adopted essentially the same wave functions here as were used in Ref. 2. The incident electron and both final electrons (1, $1'$, $2'$) are represented as plane waves:

$$\Psi_i(\vec{r}) = u(\vec{p}_i) e^{i\vec{p}_i \cdot \vec{r}} \quad (i = 1,\ 1',\ 2') , \quad (4)$$

where $u(\vec{p}_i)$ is the Dirac spinor. The bound-state wave function $\Psi_2(\vec{r})$ for an electron of quantum numbers nlm is represented by a nonrelativistic hydrogenic wave function[6]:

$$\Psi_2(\vec{r}) = \chi_{lmn}(\vec{r}) \begin{pmatrix} 1 \\ \frac{1}{2} i\alpha Z |\vec{\sigma} \cdot \vec{r}| \end{pmatrix} v . \quad (5)$$

Here $\vec{\sigma}$ is the Pauli spin vector, v the Pauli spinor, α the fine-structure constant, and Z the effective nuclear charge. Inserting the wave functions defined by Eqs. (4) and (5) in Eq. (2), we obtain

$$M = 2(2\pi)^4 e^2 \Psi_{nlm}(-\vec{p}_2) \{[(\vec{p}_1 - \vec{p}_1')^2 - (\epsilon_1 - \epsilon_2')^2]^{-1} \times \bar{u}(\vec{p}_2')\gamma_\mu u_B(\vec{p}_2) \bar{u}(\vec{p}_1')\gamma_\mu u(\vec{p}_1)\} , \quad (6)$$

where $-\vec{p}_2 = \vec{p}_1 - \vec{p}_1' - \vec{p}_2'$ represents the momentum transferred to the rest of the atom apart from the ejected electron. The spinor $u_B(\vec{p}_2)$ comes from the bound state and is the momentum representation of the spin part of the wave function given by Eq. (5), i.e.,

$$u_B(\vec{p}_2) = \begin{pmatrix} 1 \\ \frac{1}{2} i \vec{\sigma} \cdot \vec{p}_2 \end{pmatrix} v_2 , \quad (7)$$

and is formally identical to the spinor of a nonrelativistic particle with momentum $\vec{p}_2$. The wave function $\Psi_{nlm}(-\vec{p}_2)$ is the spin-independent part of the hydrogenic wave function given by Eq. (5) in momentum space and is obtained by the Fourier trans-

form

$$\Psi_{nlm}(\vec{p}_2) = (2\pi)^{-3} \int d\vec{r}\, e^{-\vec{p}_2' \cdot \vec{r}} \chi_{nlm}(\vec{r}) \ . \tag{8}$$

The cross section for ionization of an electron with quantum numbers nlm is, then,

$$\frac{d\sigma_{nlm}}{dE_1' d\Omega_1'} = \frac{(2\pi)^3 p_1' p_2' e^4}{p_1} \int d\Omega_2' |\Psi_{nlm}(-p_2)|^2 \times \left(\frac{A}{(P_1 - P_1')^4} + \frac{B}{(P_1 - P_2')^4} + \frac{2C}{(P_1 - P_1')^2 (P_2 - P_2')^2} \right) , \tag{9}$$

where

$$A = 2[(P_1 \cdot P_2')(P_1' \cdot P_2) + (P_2 \cdot P_1)(P_1' \cdot P_2') + (P_1 \cdot P_1') + (P_2 \cdot P_2') + 2] , \tag{10a}$$

$$B = 2[(P_2 \cdot P_1)(P_1' \cdot P_2') + (P_2 \cdot P_2')(P_1' \cdot P_1) + (P_1 \cdot P_2') + (P_2 \cdot P_1') + 2] , \tag{10b}$$

$$C = [2(P_2 \cdot P_1)(P_1' \cdot P_2') + (P_2 \cdot P_1) + (P_2 \cdot P_2') + (P_2 \cdot P_1') + (P_1 \cdot P_1') + (P_1' \cdot P_2') + (P_1 \cdot P_2') + 2] . \tag{10c}$$

In Eqs. (9) and (10), $P_i = (\vec{p}_i, \epsilon_i)$ are four-momenta satisfying momentum conservation

$$P_1 + P_2 = P_1' + P_2' \ . \tag{11}$$

Note that $P_2 = (\vec{p}_2, 1 - I)$ is not on the energy shell.

A further reduction of Eq. (9) can be made by treating the average momentum dependence of each electron in a particular shell. For closed shells using hydrogenic wave functions the average momentum distribution for a shell of principal quantum number n has the same form as for $n = 1$ (K shell)[7]:

$$\sum_{l,m} |\Psi_{nlm}(\vec{q})|^2 = 2n^5 |\Psi_{100}(n\vec{q})|^2 \ . \tag{12}$$

Using Eq. (11) we define an average momentum distribution for shell n containing $2n^2$ electrons as

$$\sum_{l,m} \frac{|\Psi_{nlm}(\vec{q})|^2}{2n^2} = n^3 |\Psi_{100}(n\vec{q})|^2 = \left(\frac{a_n}{\pi}\right)^5 \frac{1}{(q^2 + a_n^2)^4} \ . \tag{13}$$

The last relation in Eq. (13) follows from the fact that

$$\Psi_{100}(n\vec{q}) = \left(\frac{Z}{\pi}\right)^{5/2} \frac{1}{(n^2 q^2 + Z^2)^2} = \left(\frac{a_n}{\pi}\right)^{5/2} n^{3/2} \frac{1}{(q^2 + a_n^2)^2} \ , \tag{14}$$

where

$$a_n = Z/137n \ .$$

Use of Eq. (13) in Eq. (9) makes it possible to carry out the integration over solid angle $d\Omega_2'$. In order to obtain an expression usable for cross-section computations all quantities contained in Eq. (3) must be expressed in terms of the independent variables E_1 (initial kinetic energy), E_1' (final kinetic energy), and $\mu = \cos\theta$ (θ is the scattering angle). This reduction is done in the Appendix. The final result is of the form

$$\frac{d\sigma_n}{dE_1' d\Omega_1'} = \frac{32\pi^4 e^4 p_1' p_2'}{p_1} \times \int_{-1}^{1} dx\, F(x, \mu, E_1, E_1', a_n) G(x, \mu, E_1, E_1') \tag{15}$$

for a single electron in shell n. The function $F(x, \mu, E_1, E_1', a_n)$ is simply the quantity given by Eq. (13), i.e.,

$$F = \left(\frac{a_n}{\pi}\right)^5 \frac{1}{(p_2^2 + a_n^2)^4} = \left(\frac{a_n}{\pi}\right)^5 \frac{1}{[(q^2) + p_2'^2 + a_n^2 - 2qp_2'x]^4} \ , \tag{16}$$

where the variables $\vec{p}_1$, $\vec{p}_1'$, and $\vec{p}_2'$ can be obtained from E_1, E_1', and μ, respectively, via the conservation relations (1) and (11). $\frac{1}{2}a_n^2$ is the binding energy for an average electron in the nth shell and $q = |\vec{p}_1 - \vec{p}_1'|$ is the momentum transferred by the incident electron. The function $G(x, \mu, E_1, E_1')$ is the same for every shell and is given explicitly in terms of μ, E_1, and E_1' in the Appendix. The integration in Eq. (15) runs over $x = \cos\delta$ (where δ is the angle between the momentum-transfer vector $\vec{q} = \vec{p}_1 - \vec{p}_1'$, taken as polar axis, and $\vec{p}_2'$). This final integration must be performed numerically.

In order to evaluate Eq. (15) some choice must be made for an effective value of Z for each shell. We have used Slater's rules[8] according to which the binding energy is given by

$$\tfrac{1}{2}a_n^2 \cong I_b = \tfrac{1}{2}(Z - s)/137n^{*2} \ . \tag{17}$$

For purposes of estimating the average momentum distribution there are two problems associated with using this procedure. First, d and f electrons see much less effective charge than s and p electrons in the same shell. Second, the elements we are treating (C, Cu, Au) all contain incomplete outer shells. We have dealt with these difficulties by using the form of Eq. (13) for the momentum distribution in each subshell but have treated d and f electrons in Cu and Au as separate subshells with the appropriate values of s and n^*. The L shell in carbon has been treated by assuming its momentum distribution is given by Eq. (13) with the appropriate screening parameters ($n^* = 2$ $s = 2.75$). The valence electrons for Cu and Au have been treated as "extra" $3d$ and $5d$ electrons, respectively. Values of s and n^* used in the computations are given in Table I.

TABLE I. Slater screening parameters for Cu and Au used in Eq. (15).

nl	n^*	s
$1s$	1	0.3
$2s$, $2p$	2	4.15
$3s$, $3p$	3	11.25
$3d$	3	21.15
$4s$, $4p$	3.7	25.05
$4d$	3.7	39.5
$4f$	3.7	50.9
$5s$, $5p$	4	57.6
$5d$	4	71.5

The theoretical developments given above are similar to those made in Ref. 2 but with the following differences. In Ref. 2 the authors' main interest was in the low-energy electrons ejected at large angles in cases when the incident energy was much higher than the binding energy. In treating such cases they were able to make a number of simplifying assumptions. This included (a) evaluating only the term containing $1/(P_1 - P_2')^4$ in Eq. (9) for a scattering angle $\theta_2' \approx 0$, (b) neglecting all terms of order $1/P_1$, and (c) evaluating the cross section only for K-shell electrons. Here, since we are interested in much lower incident energies and also in the energy spectrum over the entire range, we have made no assumptions except that the momentum distribution of each bound electron is of the form given by Eq. (11).

Most of the theoretical work on ionization in the range above 100 keV has been devoted to evaluation of the total ionization cross section.[9-11] Since the bulk of the total cross section comes from small momentum transfers the theory develops along different lines from the matrix element of Eq. (2). Most of this total ionization cross-section work is done within the framework of Born approximation, which in this context means using plane waves for the initial and final states of electron 1 in the matrix element and ignoring exchange effects (i.e., not antisymmetrizing the matrix element). Both of these approximations appear justified in computing total cross sections since the main contributions to the cross section will be due to large impact parameters (small momentum transfer). Hence, provided the incident energy is several times the binding energy, exchange effects are small. However, the work on total cross sections is superior to that of either this paper or Ref. 2 since more realistic wave functions for initial and final states of the bound (or ionized) electron can be used in these calculations.

Recently theoretical work[12] on differential ionization cross sections similar to ours has appeared. The major difference is that in Ref. 12 the attention is directed towards coincidence processes in which both (scattered and ejected) electrons are observed simultaneously. Accordingly, these authors do not integrate over the momentum of one of the final-state electrons and in addition confine their treatment to nonrelativistic energies. Apart from these differences the two approaches are identical.

Our choice of wave functions represents an initial attempt to assess the effects of binding the Møller scattering. However, we expect the treatment to be inadequate at very low or very high final energies since for these cases one of the electrons has a low kinetic energy, and Coulomb rather than plane waves should be used to describe it. The effects of Coulomb forces have been considered for low energies and large scattering angles[3] to first order and found to be appreciable. In this work we have not included these effects although in Sec. V we make an estimate of how large the errors in our calculations are likely to be due to their neglect.

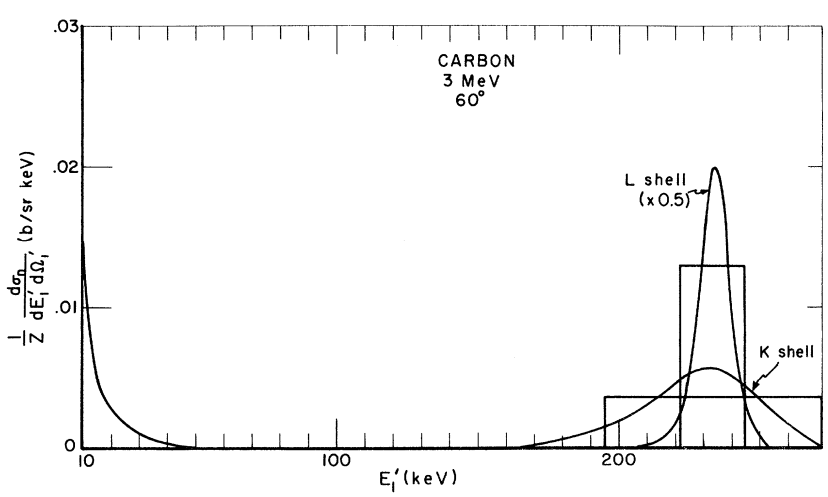

FIG. 1. K- and L-shell contributions to $(1/Z)(d\sigma/dE_1' d\Omega)$ (b/atom sr keV) for scattering at 3-MeV incident energy at 60° on carbon, showing the Møller peak at ~235-keV scattered energy (E_1') and the low-energy "tail" below 50 keV.

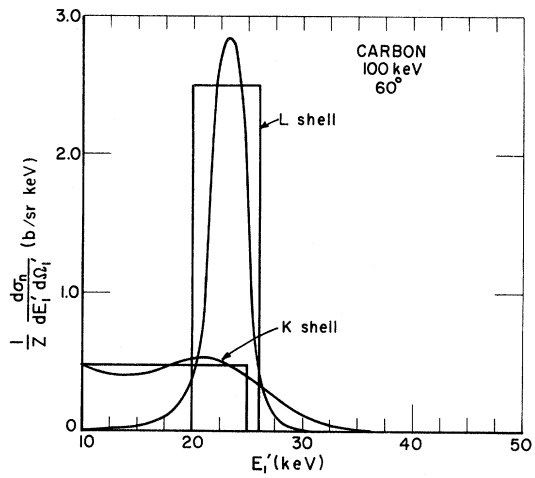

FIG. 2. K- and L-shell contributions to $(1/Z)(d\sigma/dE_1' d\Omega)$ for scattering at 100-keV incident energy at 60° on carbon.

III. CROSS-SECTION CALCULATIONS FOR ($Z=6$)

The experimental results for carbon given in Ref. 4 show that at large incident energies and large scattering angles the spectral distribution may be resolved into two contributions. One of these is a peak at the Møller energy given by

$$E_m = \frac{E_1 \cos^2\theta}{1+\frac{1}{2}E_1 \sin^2\theta} \quad . \tag{18}$$

The other contribution is a low-energy component which occurs generally at energies below 50 keV, rises steeply with decreasing final energy, and cannot be separated from the "Møller peak" for small angles of scattering or low incident energies. Our calculations show the same behavior. In Fig. 1 we show the individual K- and L-shell contributions to the spectra for scattering at 3 MeV and 60° and in Fig. 2, the spectra at 100 keV and 60°. Several things are apparent from these results. The low-energy contribution (at least for final energies above 10 keV) is due almost entirely to scattering from the K shell. At high incident energies the two contributions are well resolved, and furthermore the contributions in the Møller peak are approximately equal to the Møller cross section for the given shell. The effect of the momentum distribution of the bound electron is to broaden both K- and L-shell distributions. No deviation of the peak energy from the Møller energy given by Eq. (16) is apparent since the K- and L-shell binding energies are smaller than 1 keV for carbon. We have shown the individual Møller contributions for K- and L-shell scattering in Figs. 1 and 2 as constant cross sections of arbitrary width in order to illustrate that the area under the peaks is approximately equal to the Møller cross section for both K- and L-shell contributions.

A comparison of our results for carbon at 100, 200, and 400 keV incident energy and 60° scattering with the experimental results of Ref. 4 is shown in Fig. 3. There appear to be three major differences between the experimental and computed results. First, the peak heights observed are much smaller than those calculated. While part of this is due to

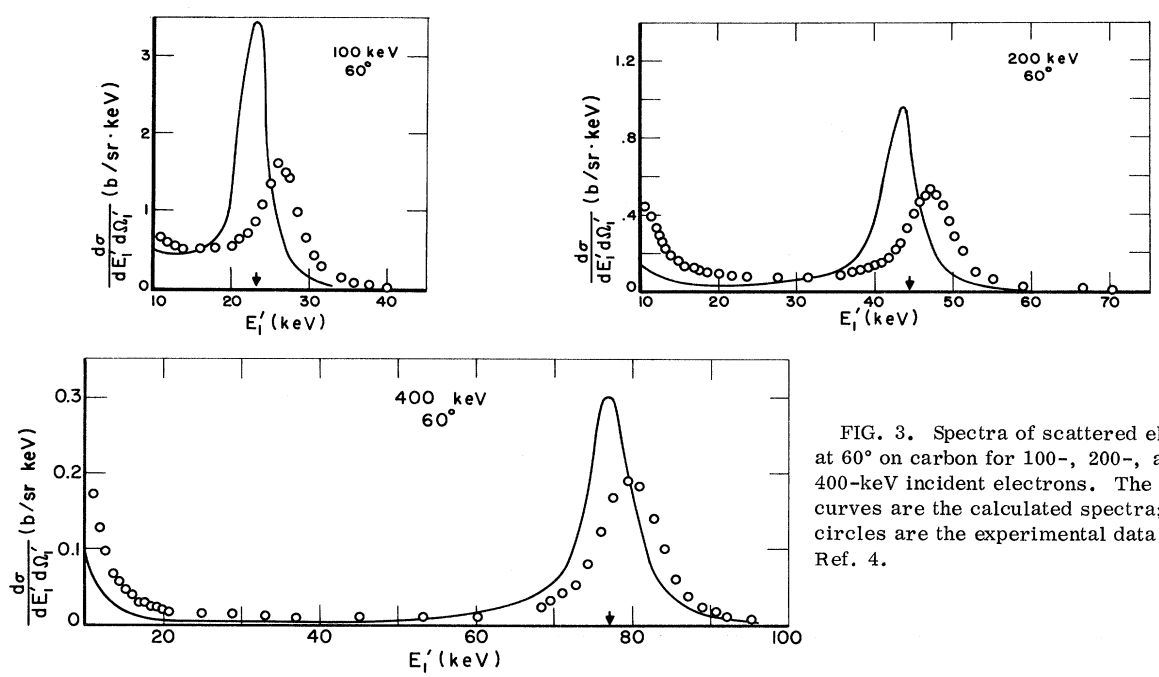

FIG. 3. Spectra of scattered electrons at 60° on carbon for 100-, 200-, and 400-keV incident electrons. The smooth curves are the calculated spectra; the circles are the experimental data of Ref. 4.

TABLE II. Contributions to Møller scattering (in b/sr) for carbon obtained by integrating over the spectral distribution of scattered electrons for given incident energy and scattering angle.

E_1'/θ		20°	40°	60°
100 keV	Møller	156	8.7	21
	calc.	146	8.6	21
	expt.	190	9.8	16
200 keV	Møller	62	3.2	6.6
	calc.	38	2.8	7.0
	expt.	42	3.3	6.3
400 keV	Møller	14	1.2	2.9
	calc.	12	1.0	2.9
	expt.	14	1.4	2.5
3 MeV	Møller			0.85
	calc.			0.85
	expt.			

instrumental broadening, the differences appear to be larger than would be expected on the basis of the 1–2-keV instrumental resolution. Second, there is a shift of approximately 3 keV toward higher energy in the measured position of the Møller peaks. Finally, the tail of the distribution at low energies is much larger than the calculations indicate and there is a larger contribution in spectral regions between the low-energy tail and the Møller peak in the experiment.

Despite the difference in spectral shapes the total energy-integrated cross section at a particular angle in both the calculations and experiment is in fairly good agreement with the Møller cross section. Table II shows a comparison between the Møller experimental and calculated cross sections. The integrated values presented here are somewhat uncertain at low scattering energies or small angles for both experiment and calculated values since the tail and peak contributions tend to merge. The procedure adopted to obtain integrated values was to use only the peak contribution, provided it could be separated from the low-energy contribution, and otherwise to arbitrarily extend the integration only to 10 keV on the low-energy side. The table indicates the integrated theoretical and experimental cross sections are approximately the same and agree with the Møller values to within about 20–30%.

In the vicinity of the Møller energy it is not necessary to carry out the calculations in full detail. The reason for this is that near the Møller energy most of the contribution to the integrand in Eq. (9) comes from values of $p_2 \ll a_n$. Thus provided $|p_1|$, p_1', and $|p_2'|$ are all much larger than a_n it is a good approximation to set $p_2 = 0$ in the large parentheses in Eq. (9). When this is done Eq. (15) reduces to

$$\frac{d\sigma_n}{dE_1' d\Omega_1'} = \frac{8a_n^5 p_1' e^4}{3\pi p_1 q}\left(\frac{1}{[(q-p_2')^2+a_n^2]^3} - \frac{1}{[(q+p_2')^2+a_n^2]^3}\right)$$

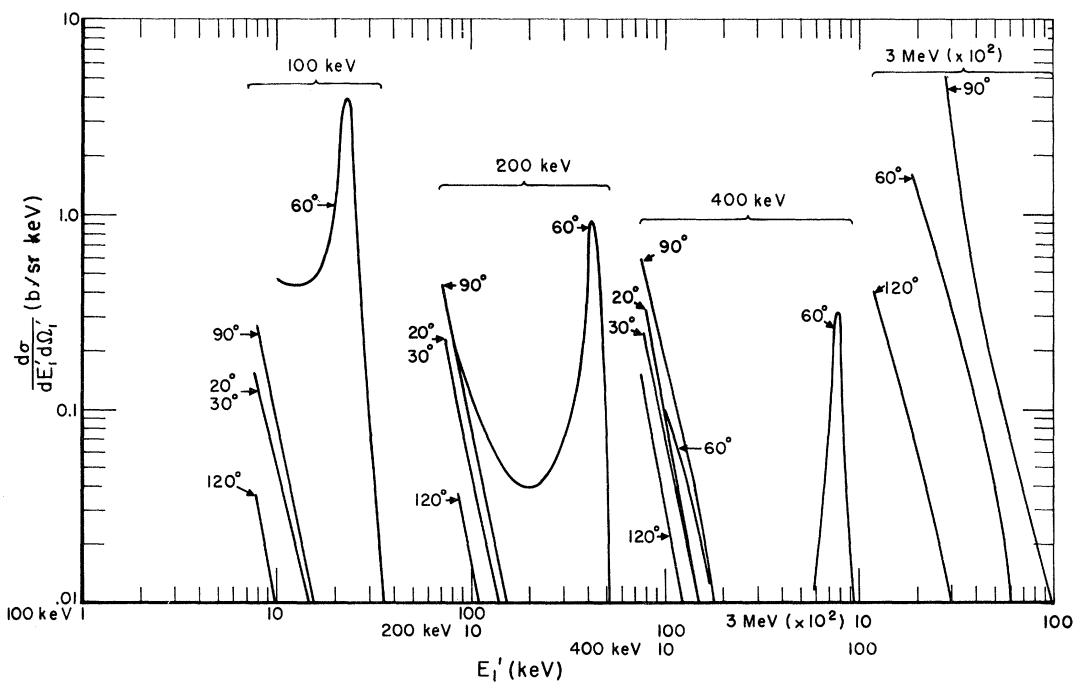

FIG. 4. Low-energy spectra at various angles for scattering on carbon for 100-, 200-, 400-keV, and 3-MeV incident electrons.

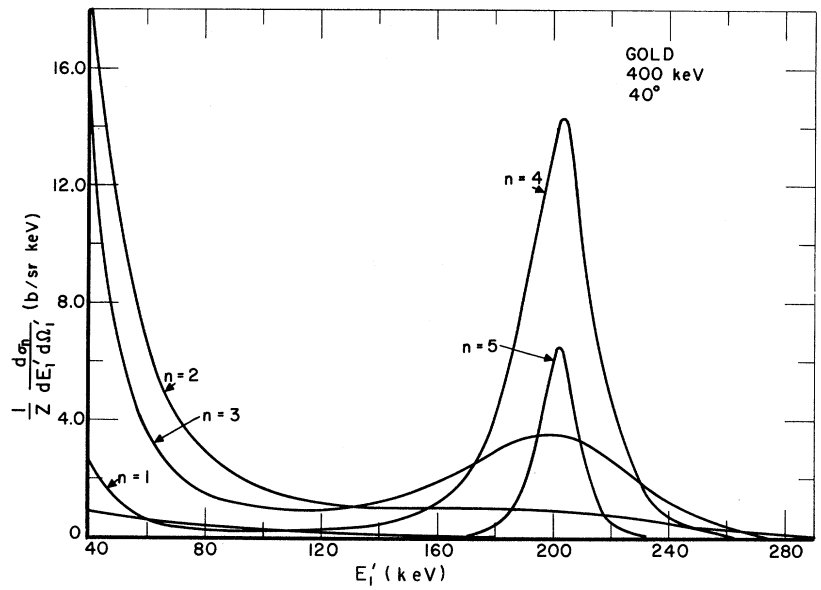

FIG. 5. Individual shell contributions to scattering from gold for 400-keV electrons at 40°.

$$\times\left[(E_1+1)^2\left(\frac{1}{E_1'^2}+\frac{1}{E_2'^2}\right)-\frac{2E_1+1}{E_1'E_2'}+1\right]. \tag{19}$$

Equation (19) was evaluated numerically for all cases where the full calculations of Eq. (15) were carried out. It was found that Eq. (19) was adequate to represent the cross section near the Møller peak (to within 5 or 10% accuracy) in all cases. However, this simpler form cannot be used for very low or very high (near E_1) final energies. Use of Eq. (19) underestimates the low-energy tail at energies above 10 keV and overestimates the cross section for values of E_1' close to E_1. This is not surprising since Eq. (19) diverges for $E_1'=E_1$ and for $E_1'=0$.

Calculations of the low-energy electron spectra have been made for all of the experimental cases treated in Ref. 4. These data have been plotted in Fig. 4 on a log-log plot similar to Figs. 10–13 of Ref. 4. The results show the same general behavior for the angular dependence of low-energy electrons as a function of incident energy as experiment. Note that the peak cross section is at about 60° for 100-keV electrons but shifts towards 90° with increasing incident energy. The calculated cross sections at a given energy and angle are generally about a factor of 2 smaller than those measured. The discrepancy between calculation and experiment is largest at 120° where the calculated cross sections are always much smaller than at 30°. In the ex-

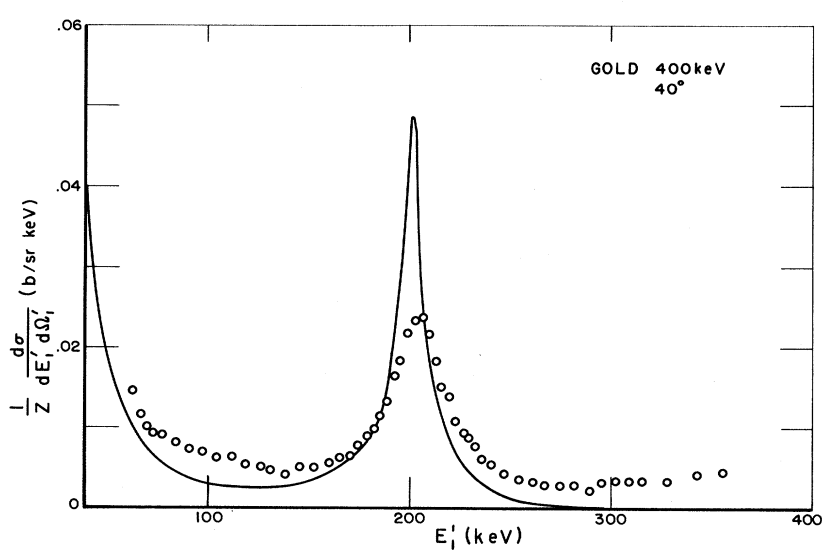

FIG. 6. Calculated and observed spectra for scattering from gold at 40° for 400-keV incident electrons. The smooth curve is the calculated spectra; the circles are the experimental data of Ref. 4.

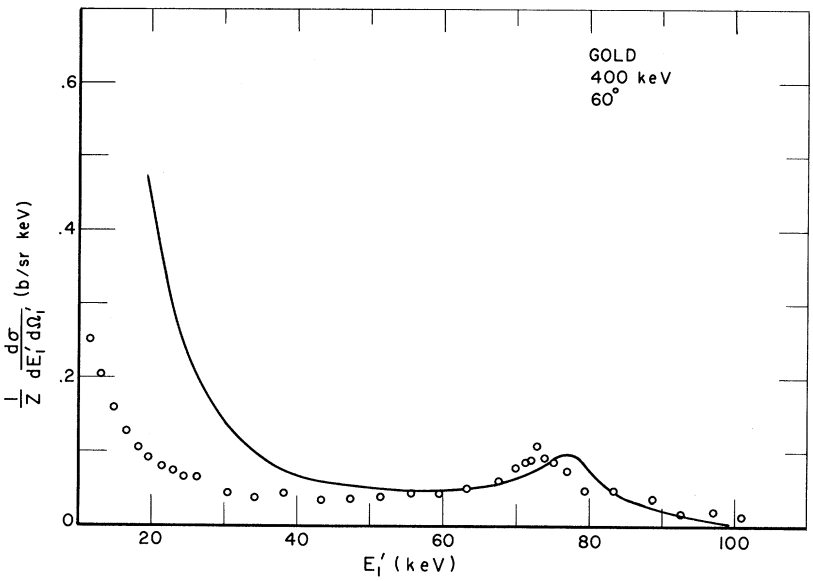

FIG. 7. Calculated and observed spectra for scattering from gold at 60° for 400-keV incident electrons. The smooth curve is the calculated spectra; the circles are the experimental data of Ref. 4.

perimental results, spectra at 30° and 120° have comparable values.

IV. CROSS SECTIONS FOR Cu(Z = 29) AND Au(Z = 79)

The spectra for scattering at a given angle for heavier elements are much more complex than that of carbon treated in the Sec. III. This complexity arises since electrons lying deep within the atom will have large binding energies and broad momentum distributions which will tend to shift the contribution to the cross section at the Møller energy towards lower energies and to broaden the spectral distribution. Figure 5 shows the calculated spectral distribution of scattered electrons from the various shells in gold at 40° with 400-keV incident energy.[13] The figure indicates the effects of binding on the spectra. For K-shell electrons there is practically no contribution to the scattering at the Møller energy but only a low-energy component. The major components of the low energy "tail," however, come from the $n = 2(L)$ and $n = 3(M)$ shells. The M-shell contribution near the Møller energy is the first shell to show evidence of a peak in that spectral region. The peak is shifted to lower energy but the binding energy (~3 keV) is so small that the shift is not striking. The outer shells $n = 4$, and 5 behave almost as free electrons (broadened by their momentum distributions) and contribute approximately to the total cross section in the ratio of the number of electrons contained in the shell $\frac{32}{19}$. Note, however, that a low-energy contribution is still present for $n = 4$ (N-shell) electrons.

The spectral distribution for Au at 400-keV incidence energy and 40° is compared in Fig. 6 with the experimental data of Ref. 4. The comparison indicates that, as for the carbon data, there is considerable broadening of the Møller peak and of the low-energy tail, presumably due to plural scattering.

For a 60° angle of observation the experimental results indicate that the peak in cross section barely rises above a background contribution, which becomes larger at low energies. The calculations show the same behavior as illustrated in Fig. 7 for 400-keV incidence. In this case there is a slight (~2 keV) shift of the peak toward lower energy in the calculation and a larger shift (~6 keV) in the experimental results. The calculated low-energy contribution in gold is larger in Figs. 6 and 7 than that observed. This is true for all other cases where low-energy data are available experimentally, and would seem to indicate that for the heavier elements plural scattering tends to smear out the low-energy tail rather than to add an additional contribution.

The data of Ref. 4 indicate that for low-incident energies (100 and 200 keV) and small final angles (20°, 40°) additional peaking of the cross section occurs at energies above the Møller energy. Also, the cross section per electron is larger for copper and gold than for carbon, owing to this high energy component. The calculations do not show this effect. In all cases the spectral distribution falls off rapidly at energies above the Møller energy, and the cross section integrated over the range near the Møller peak is approximately equal to the Møller cross section. The cross sections for C, Cu, and Au are shown for 100-keV incident energy at 20° in Fig. 8. The results at 200 and 400 keV and at 40° are similar to these results and indicate that the major effect of binding is to broaden the spectral distribution near the Møller energy. None of the

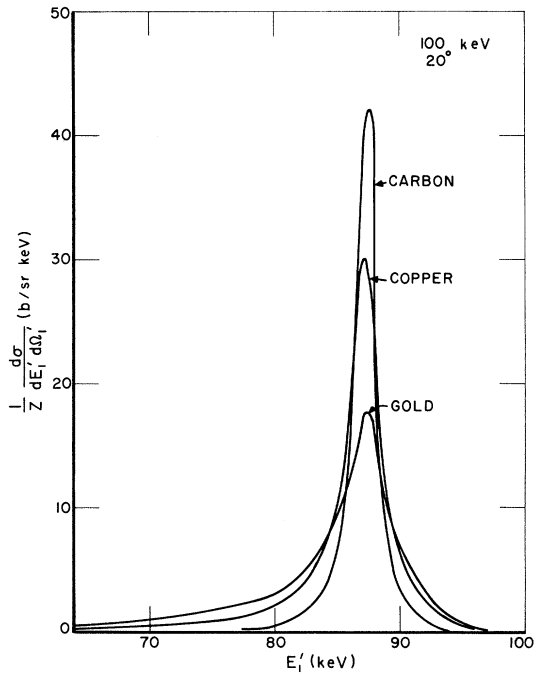

FIG. 8. Spectra for scattering of 100-keV electrons at 20° from carbon, copper, and gold.

calculations show any increase in cross section above the Møller energy so that the observation of this must either be due to plural scattering or to the fact that the plane waves used in our calculations are not sufficient to describe the scattering for cases where one of the electrons has high (and the other low) energy. For 400-keV incidence no high-energy component is present in the experimental results.

In Table III we show the integrated cross sections as calculated for Cu and Au for 20° and 40° and compare them with the Møller values. The 60° case is not included since it is impossible at that angle to separate the Møller peak value from the low-energy background. The table indicates that the cross sections are reasonably close to the Møller values even for heavy elements at low incident energies. This is surprising since, as shown in Fig. 5, the contribution for inner shells is appreciably broadened for these elements.

V. PLURAL SCATTERING AND COULOMB EFFECTS

The comparison between theory and experiment given in Secs. III and IV reveals the following discrepancies.

(a) For low-Z targets (C) the Møller peak at 60° is observed at a higher energy than calculated and the low-energy "tail" has a larger measured cross section than predicted for all angles.

(b) For larger-Z targets the Møller peak is observed at lower energies than calculated for 60° and at higher energies than calculated for 40° and 20°, and the low-energy tail has a smaller measured cross section than predicted.

(c) At low-incident energies and small scattering angles both gold and copper show large cross sections at energies above the Møller energy which are not predicted by the calculations reported here.

Although a detailed analysis of the plural-scattering effects will not be attempted a few remarks are in order. First, for the size of the foils used in the experiment (~10–60 μg/cm^2), elastic scattering following an inelastic event will always be important for low final energies (<100 keV). We attribute the discrepancies between the calculated and measured cross sections for carbon in the low-energy tails and the shift and broadening of the Møller peak observed at 60° to this effect.

For the higher-Z materials the effects of plural scattering will be even more severe both because thicker foils were used and because an electron of given energy will undergo a large average deflection in an elastic collision for a higher-Z material.

The observation of large cross sections for energies above the Møller energy observed for Cu and Au at lower energies and angles is more difficult to understand. A tentative explanation of this is that appreciable elastic scattering occurs before inelastic scattering takes place. Since the mean free path for inelastic scattering is large this would mean that the first (elastic) scattering would produce part of the angular deflection and the second (inelastic scattering) would produce a contribution at the angle of observation with energy higher than the Møller energy. One would expect an effect of this kind to be largest at low incident energies (where both inelastic and elastic cross sections are large) and at small scattering angles (where the energy loss in Møller scattering is small and thus the energy difference between inelastic and elastically scattered electrons is small). This is consistent with the experimental results.

TABLE III. Contributions to Møller scattering (inb/sr) for copper and gold obtained by integrating over the spectral distribution of scattered electrons for given incident energy and scattering angle.

E_1'	θ	20°	40°
100 keV	Møller	156	8.7
	Cu	136	···
	Au	125	8.7
200 keV	Møller	62	3.2
	Cu	91	···
	Au	38	2.4
400 keV	Møller	14	1.2
	Cu	13	···
	Au	12	1.2

In the theoretical treatment outlined in Sec. III, plane waves have been used for all electrons except the initial bound atomic electrons. Actually, the use of plane waves for slow scattered or ejected electrons is a poor choice since these electrons are actually moving in a Coulomb field of charge $\sim Z$. An estimate of the effects of replacing the plane waves in our formulation by Coulomb waves can be made as follows.

First, we assume that for high final energies (E_1') only the direct term in the scattering contributes (we ignore exchange effects). The matrix element for scattering then reduces to

$$M = \langle \Psi_0(\vec{r}_2) e^{i\vec{q}\cdot\vec{r}_2} \Psi_f(\vec{r}_2)\rangle , \tag{20}$$

where $\vec{q} = p_1 - p_1'$ is the momentum transferred in the scattering. Next, we use nonrelativistic hydrogenic wave functions corresponding to K-shell electrons for the initial-state electrons and plane waves for the final-state electrons and evaluate the square of this matrix element integrated over all angles of ejection. This may be done analytically[14] and yields the result

$$\int |M|^2 d\Omega_2' = \frac{2^5 a_n^5}{3\pi} \frac{[3(a_n^2+q^2+p_2'^2)^2+4q^2p_2'^2]}{[a_n^2+(q-p_2')^2]^3[a_n^2+(q+p_2')^2]^3} , \tag{21}$$

where p_2' is the momentum of the ejected electron.

The analogous expression for this quantity using Coulomb waves has been derived previously.[15] It is

$$\int |M|^2 d\Omega_2' = \frac{2^8 a_n^6}{3p_2'} \frac{q^2(a_n^2+3q^2+p_2'^2)\exp\{-(2a_n/p_2')\tan^{-1}[2a_np_2'/(a_n^2+q^2-p_2'^2)]\}}{(1-e^{-2\pi a_n/p_2'})[a_n^2+(q-p_2')^2]^3[a_n^2+(q+p_2')^2]^3} . \tag{22}$$

In Eqs. (21) and (22) a_n is the quantity defined by Eq. (14). Although the derivation of these equations applies only to K-shell electrons the fact that the momentum distribution is the same for all shells using screened hydrogenic wave functions means that the ratio of Eqs. (21) and (22) will provide an estimate of the effects of using Coulomb waves for the ejected electron rather than plane waves for scattering from all shells. This ratio is

$$A = \frac{(\int |M|^2 d\Omega_2')_{\text{Coulomb}}}{(\int |M|^2 d\Omega_2')_{\text{plane}}} = \frac{8\pi a_n q^2}{p_2'} \frac{a_n^2+3q^2+p_2'^2}{3(a_n^2+q^2+p_2'^2)^2+4q^2p_2'^2} \frac{\exp\{-(2a_n/p_2')\tan^{-1}[2a_np_2'/(a_n^2+q^2-p_2'^2)]\}}{1-e^{-2\pi a_n/p_2'}} . \tag{23}$$

If $q \sim p_2' \gg a_n$, then the ratio given by Eq. (23) reduces to unity. This is the condition for Møller scattering and indicates that the use of plane waves for describing the ejected electron is justified providing $p_2' \gg a_n$. However, scattering at energies well above the Møller energy corresponds to large momentum transfer q but small values of p_2'. For $q \gg a_n$, $q \gg p_2'$ the ratio in Eq. (23) is

$$A_{\substack{q\gg a_n \\ q\gg p_2'}} = \frac{8\pi a_n}{p_2'(1-e^{-2\pi a_n/p_2'})} . \tag{24}$$

Equation (24) implies that the calculations presented here will not be valid for final electron energies near the incident energy and will underestimate the cross section in this spectral range. This equation may be used to give a rough indication of the effects of Coulomb forces on our calculations. For example, for gold at 200 keV and 40° scattering the calculated cross sections at 160 keV and 180 keV final energy are 1.80×10^{-3} and 8.4×10^{-4} b/sr keV, respectively. Use of Eq. (24) leads to a different enhancement factor for the contribution of each shell, the effect being largest for the inner shells since a_n is large and p_2' small. The average enhancement factors are 16 and 40, respectively, at these energies, leading to corrected cross sections of 2.9×10^{-2} and 3.3×10^{-3} b/sr keV. These values are still lower than the experimental cross sections.

The above analysis indicates that Coulomb effects may tend to substantially increase the cross sections calculated in this paper for energies above the Møller energy, and that this effect may be responsible for the peaking observed at the high-energy side of the Møller energy for low incident energies and 20° and 40° scattering for copper and gold targets. Further analysis of this effect would require more detailed calculations using Coulomb rather than plane waves in the formulation of the equations given in Sec. III, and will not be attempted here.

APPENDIX

To perform the integration over directions of motion of the knocked-out electron, we first introduce the four-vector $Q = p_1 - p_1'$. In Eqs. (9) and (10) we then eliminate p_1' and p_2' using $p_1' = p_1 - Q$ and $p_2 = p_2' - Q$. The quantities A, B, and C are thus expressed by the four-vectors p_1, Q, and p_2' only. We choose our polar axis along the space part $\vec{q}$ of Q (i.e., along the momentum-transfer vector) and we let $\vec{p}_1$ be in the x-z plane. The direction of $\vec{p}_2'$ is specified by the polar angle $\delta = \arccos x$ and the azimuthal angle φ.

When all four-vector products are performed, the integrals over φ will all be of the standard form

$$I_{n,m}=\int_0^{2\pi}\frac{\cos^n\varphi\, d\varphi}{(w+b\cos\varphi)^m}\ , \tag{A1}$$

where n has the values 0, 1, or 2 and m the values 1 or 2. After some tedious algebra the cross section can be written as the single polar angle integral given in Eq. (15).

The function $G(x,\ \mu,\ E_1,\ E_1')$ is given by

$$G=G_1+G_2+G_3\ ,$$

where

$$G_1=(1/Q^4)\{[p_1(3y^2-1)-2qy]p_1p_2'^2x^2+[(2\epsilon_1\epsilon_2'+\tfrac{1}{2}Q^2-1)q-2(\epsilon_1+\epsilon_1')\epsilon_2'p_1y]p_2'x$$
$$+[p_1^2p_2'^2(1-y^2)+2\epsilon_1\epsilon_1'\epsilon_2'^2+\epsilon\epsilon_2'-\tfrac{1}{2}(\epsilon\epsilon_2'+1)Q^2]\}\ ,$$

$$G_2=(Y/X^{3/2})[-\epsilon\epsilon_2'(1+Q^2)+\tfrac{3}{2}Q^2+2+(1+Q^2)qp_2'x]+(1/X^{1/2})[-\tfrac{1}{2}\epsilon\epsilon_2'+\tfrac{1}{4}Q^2+\tfrac{1}{2}qp_2'x]+\tfrac{1}{4}\ ,$$

$$G_3=(1/Q^2)\{(1/X^{1/2})[\epsilon\epsilon_2'(1-Q^2)+\tfrac{1}{2}Q^2-2+(Q^2-1)qp_2'x]+[(\epsilon_1'\epsilon_2'+\tfrac{1}{2}Q^2-1)+(q-p_1y)p_2'x]\}\ ,$$

$$\epsilon_1=E_1+1,\ \epsilon_1'=E_1'+1\ ,\qquad \epsilon_2'=E_1-E_1'-I+1\ ,\qquad \epsilon=E_1-E_1'\ ,$$

$$p_i=[E_i(E_i+2)]^{1/2},\qquad q=(p_1^2+p_1'^2-2p_1p_1'\mu)^{1/2}\ ,$$

$$Q^2=2(\epsilon_1\epsilon_1'-1-p_1p_1'\mu)\ ,\qquad y=(p_1-p_1'\mu)/q$$

$$Y=2(\epsilon_1\epsilon_2'-1-p_1p_2'yx)\ ,\qquad X=a+bx+cx^2\ ,$$

$$a=4[\epsilon_1-\epsilon_2')^2+(p_1p_2'y)^2]\ ,\quad b=-8(\epsilon_1\epsilon_2'-1)p_1p_2'y\ ,\quad c=4p_1^2p_2'^2\ .$$

Note that G_1 gives the contribution from the direct term of the scattering amplitude. G_2 correspondingly gives the contribution from the exchange term and G_3 the contribution from the interference term.

---

*Present address: University of Trondheim, Trondheim, Norway.

[1]D. G. Keiffer and G. Parzen, Phys. Rev. 101, 1244 (1956).

[2]G. W. Ford and C. J. Mullin, Phys. Rev. 110, 520 (1958).

[3]T. A. Weber, R. T. Dick, and C. J. Mullin, Phys. Rev. 130, 660 (1963).

[4]G. Missoni, C. E. Dick, R. C. Placious, and J. W. Motz, Phys. Rev. A 2, 2309 (1970).

[5]Natural units $\hbar=m=c=1$ will be used throughout this paper. With this choice energies are expressed in units of $mc^2=0.511$ MeV, momentum in units of mc, cross sections in units of $r_0^2=(e^2/mc^2)^2=7.95\times10^{-26}$ cm^2. For more details see J. W. Motz, H. Olsen, and H. W. Koch, Rev. Mod. Phys. 36, 881 (1964).

[6]H. Olsen, Kgl. Norske Videnskab. Selskabs Forh. 31, 61 (1958).

[7]V. Fock, Z. Physik 98, 145 (1935).

[8]J. C. Slater, Phys. Rev. 36, 57 (1930).

[9]E. H. S. Burhop, Proc. Cambridge Phil. Soc. 36, 43 (1940).

[10]A. M. Arthurs and B. L. Moisewitsch, Proc. Roy. Soc. (London) A247, 550 (1958).

[11]A. S. Perlman, Proc. Phys. Soc. (London) 76, 623 (1960).

[12]A. E. Glassgold and G. Ialongo, Phys. Rev. 175, 151 (1968); 186, 266 (1969).

[13]Note that the curve in Fig. 5 represents the total contribution to $(1/z)(d\sigma/d\Omega_1'\, dE_1')$ for each shell. The contribution of each electron in the subshell will be $z/2n^2$ times the cross section plotted in Fig. 5.

[14]W. W. Wetzel, Phys. Rev. 44, 25 (1933).

[15]W. F. Mott and H. W. S. Massey, *Theory of Atomic Collisions* (Oxford U.P., London, 1965), p. 490.